

NSVS 06507557; a low-mass double-lined eclipsing binary ^{*†}

Ö. Çakırlı^{1‡} and C. İbanoğlu¹

¹*Ege University, Science Faculty, Astronomy and Space Sciences Dept., 35100 Bornova, İzmir, Turkey*

Released 2009 Xxxxx XX

ABSTRACT

In this paper we present the results of a detailed spectroscopic and photometric analysis of the $V=13^m.4$ low-mass eclipsing binary NSVS 06507557 with an orbital period of 0.515 d. We obtained a series of mid-resolution spectra covering nearly entire orbit of the system. In addition we obtained simultaneous VRI broadband photometry using a small aperture telescope. From these spectroscopic and photometric data we have derived the system's orbital parameters and determined the fundamental stellar parameters of the two components. Our results indicate that NSVS 06507557 consists of a K9 and an M3 pre-main-sequence stars with masses of $0.66\pm 0.09 M_{\odot}$ and $0.28\pm 0.05 M_{\odot}$ and radii of 0.60 ± 0.03 and $0.44\pm 0.02 R_{\odot}$, located at a distance of 111 ± 9 pc. The radius of the less massive secondary component is larger than that of the zero-age main-sequence star having the same mass. While the radius of the primary component is in agreement with ZAMS the secondary component appears to be larger by about 35 % with respect to its ZAMS counterpart. Night-to-night intrinsic light variations up to $0^m.2$ have been observed. In addition, the H_{α} , H_{β} lines and the forbidden line of [OI] are seen in emission. The LiI 6708 Å absorption line is seen in most of the spectra. These features are taken to be the signs of the classic T Tauri stars' characteristics. The parameters we derived are consistent with an age of about 20 Myr according to the stellar evolutionary models. The spectroscopic and photometric results are in agreement with those obtained by theoretical predictions.

Key words: stars:activity-stars:fundamental parameters-stars:low mass-stars :binaries:eclipsing-stars:T-Tauri

1 INTRODUCTION

Low-mass stars constitute the majority of stars by number in our Galaxy. Since their lower masses with respect to the Sun they have also very low intrinsic brightness. Although the intrinsic faintness of these stars many low-luminosity stars were discovered particularly by the near-infrared sky surveys: Deep Near Infrared Survey (Delfosse et al. 1997), Two Micron All Sky Survey (Skrutskie et al. 1997), Sloan Digital Sky Survey (York et al. 2000), Northern Sky Variability Survey (Wozniak et al. 2004). Since their main-sequence lifetimes are considerably longer than the age of the universe both the young and old low-mass stars are located on the lower right part of the the HR diagram. Low-mass stars surround many important regions of stellar parameter space which include the onset of complete convection in the stellar interior, the onset of electron degeneracy in the core, and the formation of dust and depletion metals onto dust grains in the stellar atmosphere (West et al. 2004). Recent studies have shown that while the observed radii of the low-mass stars are significantly larger than those predicted by current stellar models, in contrast their effective temperatures are cooler (Ribas et al. 2008, Lopez-Morales and Ribas 2005). Chabrier, Gallardo & Baraffe (2007) have put forward the hypothesis that the observed radius and temperature discrepancies are consequences of the convection due to rotation and/or magnetic field and the presence of large surface magnetic spots. Therefore low-mass stars are key interest in studies of both formation of the stars in star-forming regions and comparison their parameters with those predicted from theoretical stellar models.

The fundamental parameters such as mass, radius, effective temperature and luminosity, all in a distance-independent manner, of a star could be determined empirically from eclipsing binary stars. Precise masses and radii can be determined from multi-wavelength photometry and spectroscopy, obtained with current technology, of double-lined close binary systems. However, the number of well-studied eclipsing binaries with low-mass components is rather small because of their low intrinsic brightness. Furthermore, most of their light curves are undergone strong distortion due to magnetic activity. Therefore, multi-passband photometric and spectroscopic observations of additional low-mass binaries would be extremely useful.

The binary nature of the star known as NSVS 06507557 (=2MASS J01582387+2521196,

* Based on photometric and spectroscopic observations collected at TÜBİTAK National Observatory (Turkey).

† Table 1 is only available in electronic form at the CDS via ftp to <http://www.blackwell-synergy.com/doi...>

‡ e-mail: omur.cakirli@ege.edu.tr

hereafter NSVS 0650) was discovered by Shaw and Lopez-Morales (2006) using the database NSVS (Wozniak et al. 2004). The eclipse period was determined to be 0.515 d. Later on the first VRI light curves and preliminary models are presented by Coughlin and Shaw (2007). Taking the BVRI magnitudes from the USNO NOMAD catalog and JHK from 2MASS catalog they estimated the effective temperature of 3860 K for the primary, corresponding to a spectral type of M0V. As they have noted a difficulty encountered in modeling was the high-level spot activity of the components. Not only the radii and effective temperatures of the component stars were determined but also the rough masses estimated by them. We have conducted a photometric and spectroscopic monitoring program of several low-mass eclipsing binaries. In this paper we present, the results of multi-wavelength optical photometry and spectroscopy for double-lined eclipsing binary NSVS 0650.

2 OBSERVATION

2.1 Photometry

NSVS 0650757 was first identified in the NORTHERN SKY VARIABILITY SURVEY (NSVS; Wozniak et al. 2004) as a detached eclipsing binary system with a maximum, out-of-eclipse V-bandpass magnitude $V=13^m.05$ and a period of $P=0.51509$ day. The data from the NSVS, obtained with the Robotic Optical Transient Search Experiment telescopes (ROTSE), contains positions, light curves and V magnitudes for about 14 million objects ranging in magnitudes from 8 to 15.5. The B, V, R, and I magnitudes for NSVS 0650 were listed in the USNO NOMAD catalog as (NAVAL OBSERVATORY MERGED ASTRONOMICAL DATASET, NOMAD-1.0, Zacharias et al. 2004), $B=14^m.53$, $V=13^m.37$, $R=12^m.47$; on the other hand the infra-red magnitudes in three bandpasses were given as $J=10^m.918$ $H=10^m.267$, and $K=10^m.092$ in the 2MASS catalog (Cutri et al. 2003).

In the NSVS survey, 262 V-bandpass measurements of the variable were obtained during the period June 1999 - March 2000 with a median sampling rate of 0.25^{-1} . The resulting light curve exhibits periodic eclipses with a depth of $\sim 0^m.7$ in the deeper eclipse and the mean standard deviation in the out-of-eclipse phases was about $0^m.073$.

The photometric observations of NSVS 0650 were carried out with the 0.4 m telescope at the Ege University Observatory. The 0.4 m telescope equipped with an Apogee 1kx1k CCD camera and standard Bessel VRI bandpasses. The observations were performed on seven nights between September 01 and November 30, 2008. To get the higher accuracy

Table 1. Differential photometric measurements of NSVS 0650 in the V, R and I bandpasses.

HJD(2 400 000+)	ΔV	HJD(2 400 000+)	ΔR	HJD(2 400 000+)	ΔI
54725.35259	1.6025	54725.35296	1.1780	54725.35326	0.5799
54725.35370	1.6304	54725.35406	1.1572	54725.35437	0.5563
...
...

the target NSVS0650 was placed near to the center of the CCD and three nearby stars located on the same frame were taken for comparison. The stars GSC 01760-01860 and USNO A2.0 1125 638990 were selected as comparison and check, respectively. Therefore the target and comparison stars could be observed simultaneously with an exposure time of 10 seconds. Since the variable is very cool, red star the signal-to-noise ratio was highest in I- and lowest in the V-bandpass. The differential observations of the comparison stars showed that they are stable during time span of our observations. The data were processed with standard data reduction procedures including bias and over scan subtraction, flat-fielding, and aperture photometry. A total of 743, 812 and 612 photometric measurements were obtained in each V, R and I bandpasses, respectively. The average uncertainty of each differential measurement was less than $0^m.030$. The V-, R- and I-bandpass magnitude differences, in the sense of variable minus comparison, are listed in Table 1 (available in the electronic form at the CDS).

The light curve shows a deep primary eclipse with an amount of $0^m.70$ in the V-bandpass and a shallow secondary eclipse with an amount of $0^m.23$ which are clearly separated in phase, as is typical of fully detached binaries. The primary and secondary eclipses occur almost 0.5 phase interval, indicating nearly circular orbit. An inspection of the nightly light curves presented in Fig. 1 clearly indicates considerable out-of-eclipse light variations up to $0^m.2$. This intrinsic variation of the binary system manifests itself in the deeper primary eclipse.

2.2 Orbital period and ephemeris

The first orbital period for NSVS 0650 was determined as $P=0.51509957$ d by Shaw and Lopez-Morales (2006) from the NSVS database. Later on Coughlin & Shaw (2007) observed seven low-mass detached systems, including NSVS 0650, with the Southeastern Association for Research in Astronomy (SARA) 0.9 m telescope. An orbital period of $P=0.5150895\pm 0.0000008$ days, and an initial epoch $T_0(\text{HJD})=2453312.3722\pm 0.0005$ for the mid-primary eclipse were calculated using a least square fit. Partial primary and secondary eclipses which were de-

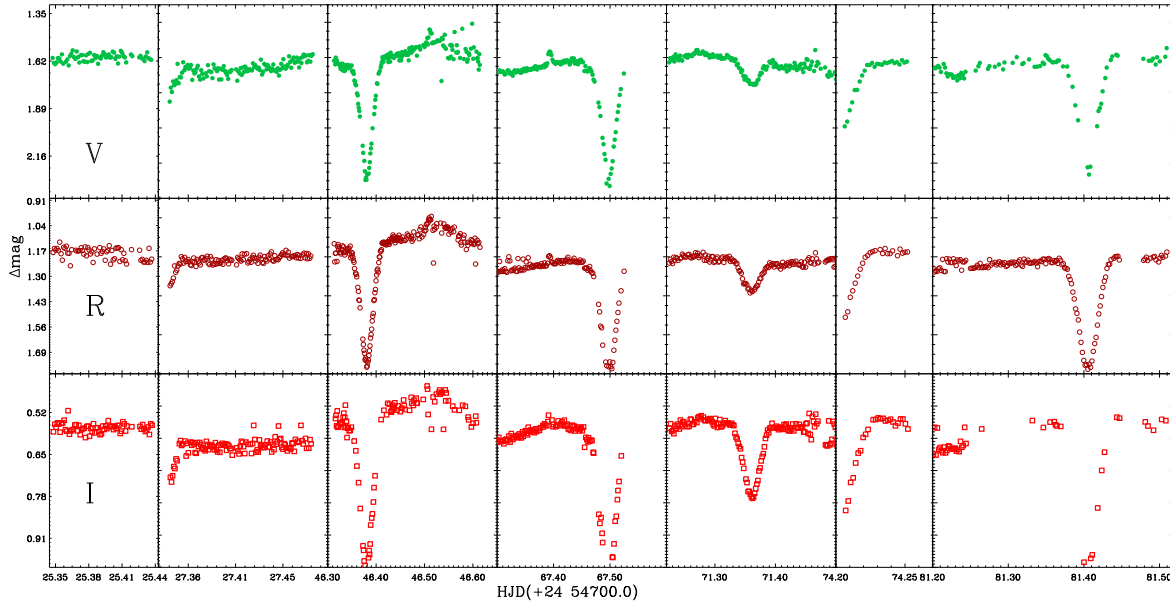


Figure 1. The V-, R-, and I-bandpass nightly light curves for NSVS 0650 from top to bottom. The V-, R-, and I-bandpass light curves clearly show that the brightness of the variable significantly varies from night to night, particularly in out of eclipse.

tected in the time series photometric data were used in combination with the NSVS photometry to derive this ephemeris for the system.

We obtained three times of mid-primary and one secondary eclipse during our observing run. The mid-eclipse timings and their standard deviations are calculated using the method of Kwee & van Woerden (1956). These timings of the eclipses were listed in Table 1 together with two primary and a secondary eclipse collected from literature. The times for mid-eclipses are the average of times obtained in three bandpasses. We define the epoch of the system, T_0 , to be the midpoint of the most complete primary eclipse. For this reason we use the V-, R-, and I-bandpass data obtained on JD=2 454 746 which cover almost the whole primary eclipse. A linear least square fit to the data listed in Table 1 yields the new ephemeris as,

$$\text{Min } I(HJD) = 24\,54746.3801(5) + 0.51508836(9) \times E, \quad (1)$$

where E corresponds to the cycle number. The residuals in the last column of Table 2 are computed with the new ephemeris. While the orbital period is nearly the same with that determined by Coughlin & Shaw (2007) its uncertainty is now very smaller than estimated by them. In the computation of the orbital phase for individual observations we used this ephemeris.

Table 2. Times of minima measured from the *VRI*-bandpass light curves.

HJD(2 400 000+)	E	Type	O-C
51537.1282**	-6230.5	II	0.0099
51581.1569**	-6145.0	I	-0.0015
53312.3722†	-2784.0	I	-0.0006
54746.3809±0.0005	0.0	I	0.0000
54767.4978±0.0006	41.0	I	-0.0018
54771.3631±0.0004	48.5	II	0.0004
54781.4056±0.0002	68.0	I	-0.0014

** From the NSVS database.

† Coughlin & Shaw (2007).

2.3 Intrinsic light variations

The light curve of NSVS 0650 shows two well-separated eclipses, as a typical of detached eclipsing binaries. The phase difference between the eclipses is about 0.5 which indicates a nearly circular orbit. Since the depths of the eclipses are very different, indicating that the components have unequal effective temperatures. The light variation both in primary and out-of-eclipse is clearly seen in all bandpasses. This light variation of about 0.2 mag peak-to-peak in the out-of-eclipse portions of the light curve reveals that there is an intrinsic variation in one or both components of the system. The amplitude of the intrinsic variations seems to larger with longer wavelengths. The light variations observed on JD 2454746 with long duration, just between primary and secondary eclipses, and also on JD 2454767 with very short duration, resemble a flare-like event which is common in M-type dwarf stars.

The data obtained by us are concentrated on seven nights ranging a time span of 56 days. The stars having masses smaller than that of the Sun are known to be heavily spotted. Therefore the out-of-eclipse light variations may be attributed to large spots on the surface of one or both component stars. In addition, flares on the less massive star cannot be ignored. However, it should be noted that the intrinsic light variations do not resemble to those observed in the spotted stars. A spot or spot groups on one or both components produces usually wave-like distortion on their light curves. However, the out-of-eclipse light variations in NSVS 0650 seem to not correlated with the orbital period.

2.4 Spectroscopy

Optical spectroscopic observations of NSVS 0650 were obtained with the Turkish Faint Object Spectrograph Camera (TFOSC) attached to the 1.5 m telescope on 3 nights (September 15, 16, and 17, 2008) under good seeing conditions. Further details on the telescope and the spectrograph can be found at <http://www.tug.tubitak.gov.tr>. The wavelength coverage of

each spectrum was 4100-8100 Å in 11 orders, with a resolving power of $\lambda/\Delta\lambda$ 7 000 at 6563 Å and an average signal-to-noise ratio (S/N) was ~ 120 . We also obtained a high S/N spectrum of the M dwarf GJ 740 (M0 V) and GJ 623 (M1.5 V) for use as templates in derivation of the radial velocities (Nidever et al. 2002).

The electronic bias was removed from each image and we used the 'crreject' option for cosmic ray removal. Thus, the resulting spectra were largely cleaned from the cosmic rays. The echelle spectra were extracted and wavelength calibrated by using Fe-Ar lamp source with help of the IRAF ECHELLE package.

The stability of the instrument was checked by cross correlating the spectra of the standard star against each other using the FXCOR task in IRAF. The standard deviation of the differences between the velocities measured using FXCOR and the velocities in Nidever et al. (2002) was about 1.1 km s^{-1} .

2.4.1 Spectral classification

We have used our spectra to reveal the spectral type of the primary component of NSVS 0650. For this purpose we have degraded the spectral resolution from 7 000 to 3 000, by convolving them with a Gaussian kernel of the appropriate width, and we have measured the equivalent widths (EW) of photospheric absorption lines for the spectral classification. We have followed the procedures of Hernández et al. (2004), choosing helium lines in the blue-wavelength region, where the contribution of the secondary component to the observed spectrum is almost negligible. From several spectra we measured $EW_{\text{HeI}+\text{FeI}\lambda 4922} = 1.18 \pm 0.12 \text{ \AA}$.

From the calibration relations EW -Spectral-Type of Hernández et al. (2004), we have derived a spectral type of K8 with an uncertainty of about 1 spectral subclass. The effective temperature deduced from the calibrations of Drilling & Landolt (2000) or de Jager & Nieuwenhuijzen (1987) is about 4 050 K. The spectral-type uncertainty leads to a temperature error of $\Delta T_{\text{eff}} \approx 300 \text{ K}$.

The catalogs USNO, NOMAD and 2MASS provides BVRIJHK magnitudes for NSVS 0650. Using the observed colors of $B-V=1.36\pm 0.02$ and $V-I=2.13\pm 0.02$ mag and color-temperature relationships given by Drilling & Landolt (2000) for the main sequence stars we estimate a spectral type $K9\pm 1$ with an effective temperature of $3930\pm 50 \text{ K}$ for the primary star. The observed infrared colors of $J-H=0.651\pm 0.043$ and $H-K=0.175\pm 0.038$ given in the 2MASS catalog (Cutri et al. 2003) correspond to a spectral type of $K9\pm 2$ is in a good agree-

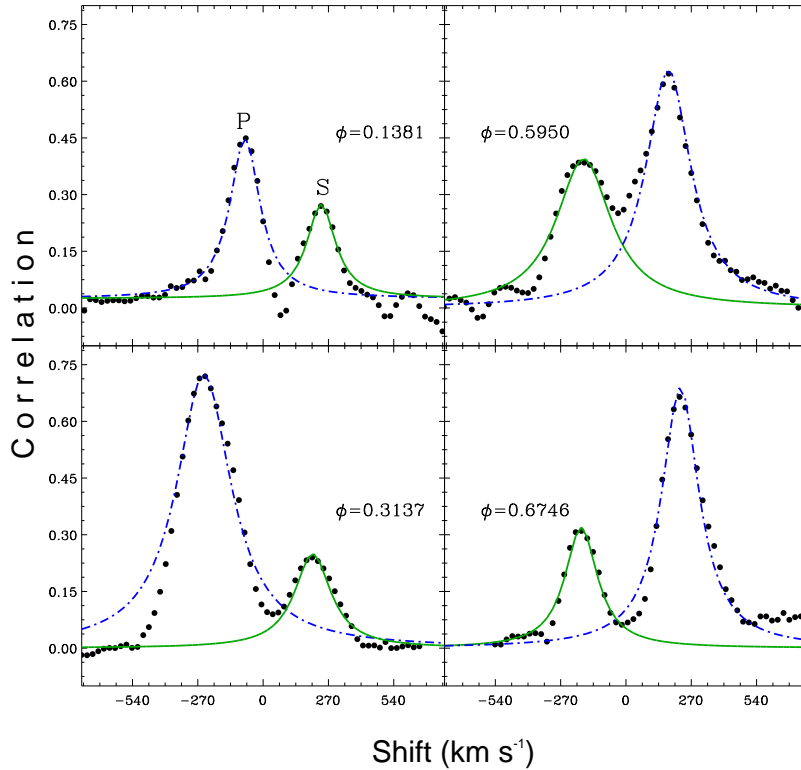


Figure 2. Sample of Cross Correlation Functions (CCFs) between NSVS 0650 and the radial velocity template spectrum around the first and second quadrature.

ment with that we derived by wide-band B-V and V-I photometric colors. We estimated a temperature of 3920 ± 175 K from the calibrations of Tokunaga (2000). Temperature uncertainty of the primary component results from considerations of spectral type uncertainties, and calibration differences. The weighted mean of the effective temperature of the primary star is 3960 ± 80 K. The effective temperature of the primary star what we derived from the photometric measurements is an a good agreement with that we estimated from the spectra alone.

3 ANALYSIS

3.1 Radial velocity curve

To derive the radial velocities for the components of binary system, the 16 TFOSC spectra of the eclipsing binary were cross-correlated against the spectrum of GJ 740, a single-lined M0V star, on an order-by-order basis using the FXCOR package in IRAF. The majority

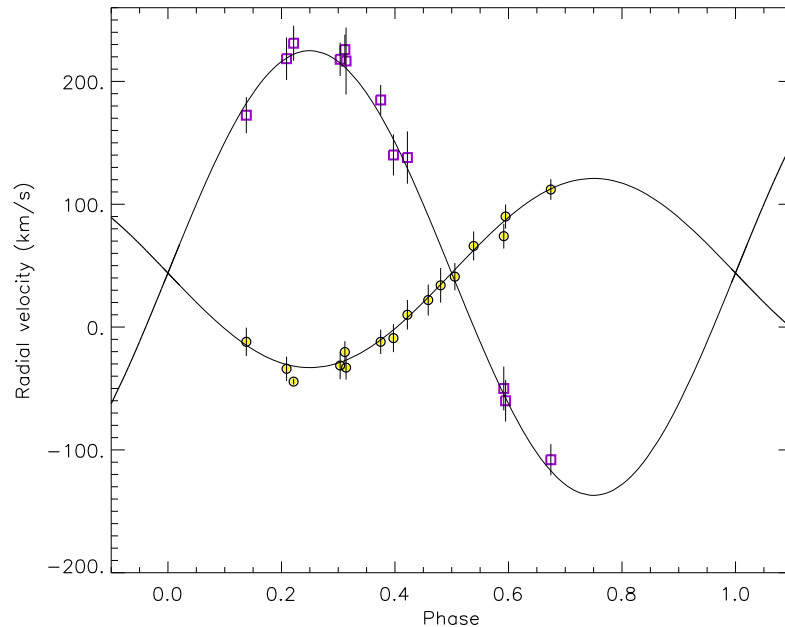


Figure 3. Radial velocity curve folded on a period of 0.51508836 days, where phase zero is defined to be at primary mid-eclipse. Symbols with error bars show the RV measurements for two components of the system (primary: open circles, secondary: open squares).

of the spectra showed two distinct cross-correlation peaks in the quadrature, one for each component of the binary. Thus, both peaks were fit independently in the quadrature with a Gaussian profile to measure the velocity and errors of the individual components. If the two peaks appear blended, a double Gaussian was applied to the combined profile using *de-blend* function in the task. For each of the 16 observations we then determined a weighted-average radial velocity for each star from all orders without significant contamination by telluric absorption features. Here we used as weights the inverse of the variance of the radial velocity measurements in each order, as reported by FXCOR. In these data, we find no evidence for a third component, since the cross-correlation function showed only two distinct peaks.

We adopted a two-Gaussian fit algorithm to resolve cross-correlation peaks near the first and second quadratures when spectral lines are visible separately. Figure 2 shows examples of cross-correlations obtained by using the largest FWHM at nearly first and second quadratures. The two peaks, non-blended, correspond to each component of NSVS 0650. The stronger peaks in each CCF correspond to the more luminous component which has a larger weight into the observed spectrum.

The heliocentric RVs for the primary (V_p) and the secondary (V_s) components are listed in Table 3, along with the dates of observation and the corresponding orbital phases com-

Table 3. Heliocentric radial velocities of NSVS 0650. The columns give the heliocentric Julian date, the orbital phase (according to the ephemeris in Eq. 1), the radial velocities of the two components with the corresponding standard deviations.

HJD 2400000+	Phase	Star 1		Star 2	
		V_p	σ	V_s	σ
54725.4190	0.3058	-41.3	11.1	218.0	13.6
54725.4800	0.4242	1.0	12.0	138.0	21.3
54725.5231	0.5079	41.0	11.1	–	–
54725.5675	0.5941	74.0	10.1	-50.0	17.8
54725.6102	0.6770	112.0	8.4	-108.0	12.7
54726.3640	0.1404	-12.0	11.5	172.5	14.7
54726.4069	0.2237	-44.4	2.4	231.1	14.2
54726.4545	0.3161	-33.0	9.8	216.6	27.3
54726.4975	0.3996	-9.0	11.4	140.1	16.7
54726.5404	0.4829	24.0	14.1	–	–
54726.5993	0.5973	90.0	9.8	-60.0	16.9
54727.4307	0.2114	-34.0	9.9	218.5	17.3
54727.4836	0.3141	-20.3	8.8	225.9	12.2
54727.5161	0.3771	-12.0	9.9	184.9	12.2
54727.5593	0.4610	22.0	12.6	–	–
54727.6005	0.5410	66.0	11.8	–	–

puted with the new ephemeris given in §2.2. The velocities in this table have been corrected to the heliocentric reference system by adopting a radial velocity of 9.5 km s^{-1} for the template star GJ 740. The RVs listed in Table 3 are the weighted averages of the values obtained from the cross-correlation of orders #4, #5, #6 and #7 of the target spectra with the corresponding order of the standard star spectrum. The weight $W_i = 1/\sigma_i^2$ has been given to each measurement. The standard errors of the weighted means have been calculated on the basis of the errors (σ_i) in the RV values for each order according to the usual formula (e.g. Topping 1972). The σ_i values are computed by FXCOR according to the fitted peak height, as described by Tonry & Davis (1979).

First we analysed the radial velocities for the initial orbital parameters. We used the orbital period held fixed and computed the eccentricity of the orbit, systemic velocity and semi-amplitudes of the RVs. The results of the analysis are as follows: $e=0.002\pm 0.001$, i.e. formally consistent with a circular orbit, $\gamma=44\pm 6 \text{ km s}^{-1}$, $K_1=77\pm 3$ and $K_2=181\pm 12 \text{ km s}^{-1}$. Using these values we estimate the projected orbital semi-major axis and mass ratio as: $a \sin i = 2.63\pm 0.12 R_\odot$ and $q = \frac{M_2}{M_1} = 0.425\pm 0.044$.

3.2 Light curve modeling

As we noted in Section 2.3 the light curve of the system is considerably distorted due to light fluctuations both at maxima and in the deeper primary minimum. The largest distortion with longest duration was observed on JD 24 54746. Neither the amplitude nor the period

Table 4. Results of the V-, R-, and I-bandpass light curve analysis for NSVS 0650. The adopted values are the weighted means of the values determined from the individual light curves.

Parameters	V	R	I	Adopted
i°	83.5±0.2	86.5±1.3	81.7±0.6	83.3±0.6
T_{eff1} (K)	3960[Fix]	3960[Fix]	3960[Fix]	3960[Fix]
T_{eff2} (K)	3269±51	3401±43	3412±48	3365±48
Ω_1	4.847±0.091	4.738±0.90	4.982±0.145	4.886±0.090
Ω_2	3.735±0.035	4.151±0.061	3.740±0.090	3.830±0.067
r_1	0.228±0.005	0.231±0.005	0.224±0.007	0.227±0.006
r_2	0.176±0.003	0.148±0.004	0.171±0.006	0.167±0.005
$L_1/(L_1 + L_2)$	0.889±0.014	0.866±0.010	0.785±0.020	—
χ^2	1.345	1.858	0.880	—

^a See §2.1.2

or cycle of these intrinsic variations are known at this step. Therefore, we take all the available V-, R- and I-bandpass data for the orbital parameter analysis. The differential magnitudes of 743 in V-, 812 in R- and 612 in I-bandpass were converted to intensities using the differential magnitudes at out-of-eclipses as $\Delta V=1^m.648\pm 0^m.003$, $\Delta R=1^m.198\pm 0^m.001$, $\Delta I=0^m.575\pm 0^m.002$.

We used the most recent version of the eclipsing binary light curve modeling algorithm of Wilson & Devinney (1971) (with updates), as implemented in the PHOEBE code of Prša & Zwitter (2005). The code needs some input parameters, which depend upon the physical structures of the component stars. In the light curve solution we fixed some parameters whose values can be estimated from global stellar properties, such as effective temperature and mass of the star. Therefore we adopted the linear limb-darkening coefficients from Van Hamme (1993) as 0.39 and 0.28 for the primary and secondary components, respectively; the bolometric albedos from Lucy (1967) as 0.5, typical for a fully convective stellar envelope, the gravity brightening coefficients as 0.32 for the both components. The rotation of components is assumed to be synchronous with the orbital one. The mass-ratio of 0.425 was adopted from the semi-amplitudes of the radial velocities. We started the light curve analysis with an effective temperature of 3960 K for the primary star of NSVS 0650. The adjustable parameters in the light curves fitting were the orbital inclination, the surface potentials, the effective temperature of secondary, the luminosity of the primary.

Using a trial-and-error method we obtained a set of parameters, which represented the observed light curves. A detached configuration, MODE 2, with coupling between luminosity and temperature was chosen for solution. The iterations were carried out automatically until convergence, and solution was defined as the set of parameters for which the differential corrections were smaller than the probable errors. The orbital and stellar parameters from

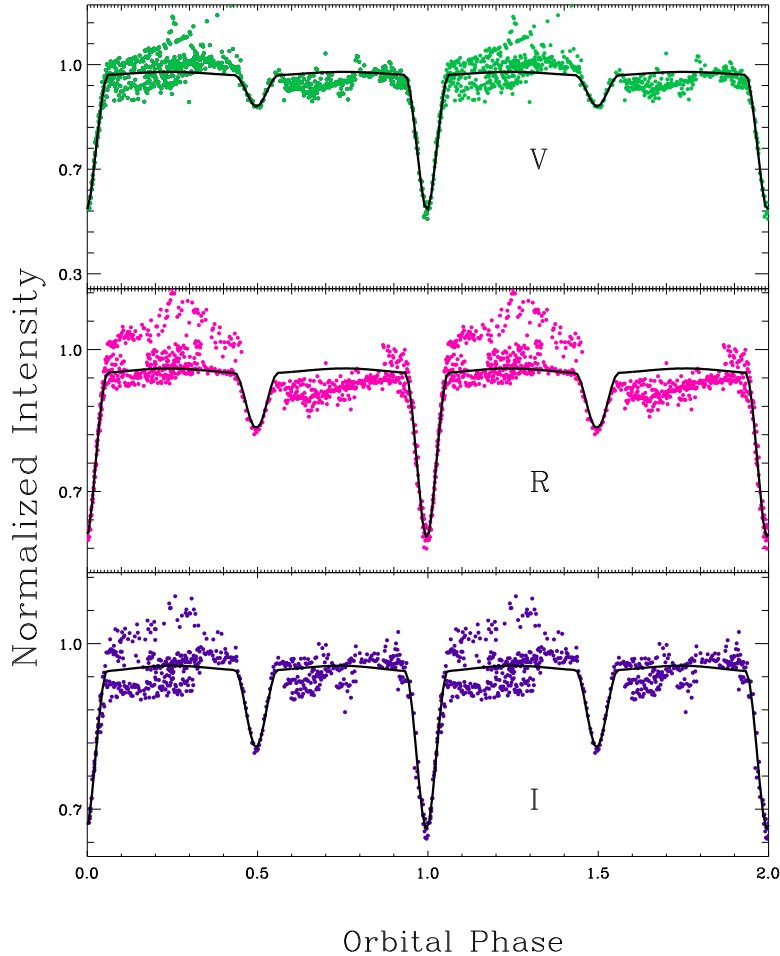


Figure 4. The phase folded VRI light curves for NSVS 0650. The best fitting solutions represented by the solid lines are also plotted for comparison (see text).

the V-, R- and I-bandpass light and radial velocity curves analysis are listed in Table 4. The uncertainties given in this table are taken directly from the out-put of the program. The computed light and velocity curves corresponding to the individual light-velocity solutions are compared with the observations in Figs. 3 and 4.

4 THE SPECTRUM

NSVS 0650 has a complex spectrum over the wavelength interval from ~ 4100 to 8100 \AA . The spectrum is dominated by forbidden lines and to a smaller degree, permitted emission lines of neutral metals. Strong and broad double-peaked H_α , H_β and [OI] lines are present, with the peak separation in H_α larger than the higher *Balmer lines*. The presence of the strong Li

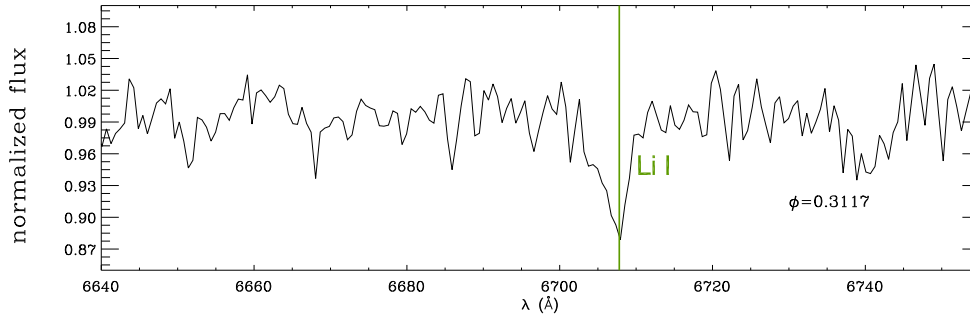


Figure 5. The composite spectrum in the spectral region containing the Li I 6708 Å line observed on JD 24 54727.4836.

6708 Å absorption line can serve as a reliable youth indicator of a star, as evidenced in the case of NSVS 0650. Young, low-mass pre-main-sequence stars are called T Tauri stars (TTS). They present the following characteristics: 1) Emission line spectra, 2) Presence of forbidden narrow-lines such as [OI], [NII] and [SIII], 3) Photospheric continuum excesses (Barrado y Navascues and Martin, 2003). TTSs are classified into two sub-groups, the classical T Tauri stars (cTTSs) and the weak-lined T Tauri stars (wTTSs). A cTTS is surrounded by an optically thick disk from which it accretes material. Whereas a wTTS represents the final stage of accretion and disc-clearing processes (Bertout et al. 2007, Schisano et al. 2009). The equivalent width of H_{α} emission is used as an empirical criterion to distinguish between cTTS and wTTS, being smaller in the latter. Due to possible variability, no clean cut can be defined between the cTTS and wTTS based on the H_{α} emission alone.

Spectral and photometric properties and night-to-night light variability of NSVS 0650 indicate that the active star in the system resembles many characteristics of the TTSs as given above and discussed by Alcalá et al. (1993), Covino et al. (1996), and Alencar & Basri (2000). As it is known the optical emission lines are definite characteristics of the many late type, main-sequence systems, including NSVS 0650. Another fundamental characteristic of TTSs is the variations of H-line profiles (Ferro & Giridhar 2003). NSVS 0650 is composed of low-mass stars which cover most of the properties of the T Tauri stars.

4.1 Line profiles

The most conspicuous line with dramatic profile variations in the system’s spectrum appears to be the H_{α} . The H_{α} line is the most prominent feature in the spectra of TTSs. The presence of the Li absorption line at 6708 Å (see Fig. 5, for an example) and weak H_{α} in emission leads us to classify the star as weak-lined T Tauri star. In Figure 6 we display the H_{α} line

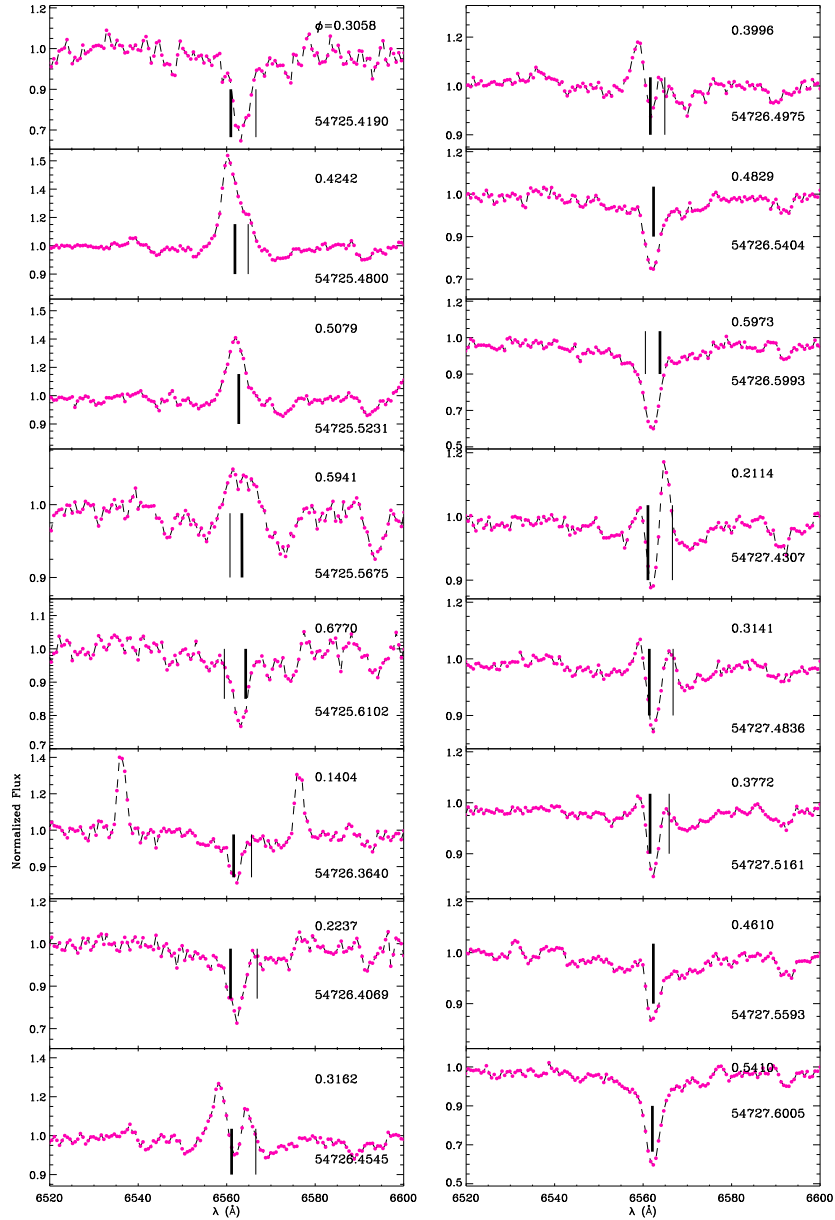


Figure 6. Variation of the H_{α} line profiles of NSVS 0650. The normalized spectrum at the H_{α} ordered with the orbital phase. The vertical thick and thin lines show the rest wavelengths corresponding to the primary and secondary component photospheres, respectively.

region observed at various orbital phases in three consecutive nights. Each spectrum has been normalized to the continuum. Julian date and the orbital phase for each observation are given in each panel. On JD 2454725 the H_{α} line appears to be a single, shallow absorption, i.e., filled-in by emission, at orbital phase of about 0.3058. At orbital phases of 0.4242, 0.5079 and 0.5939 the same line becomes single, emission above the continuum and at phase of 0.6770 it turns to be an absorption again. On JD 2454726, the following night, the H_{α} line is seen as single absorption at phases of 0.1404 and 0.2237, whereas double-peaked emission profiles at phases of 0.3162 and 0.3996, but it turns to absorption in a short time interval

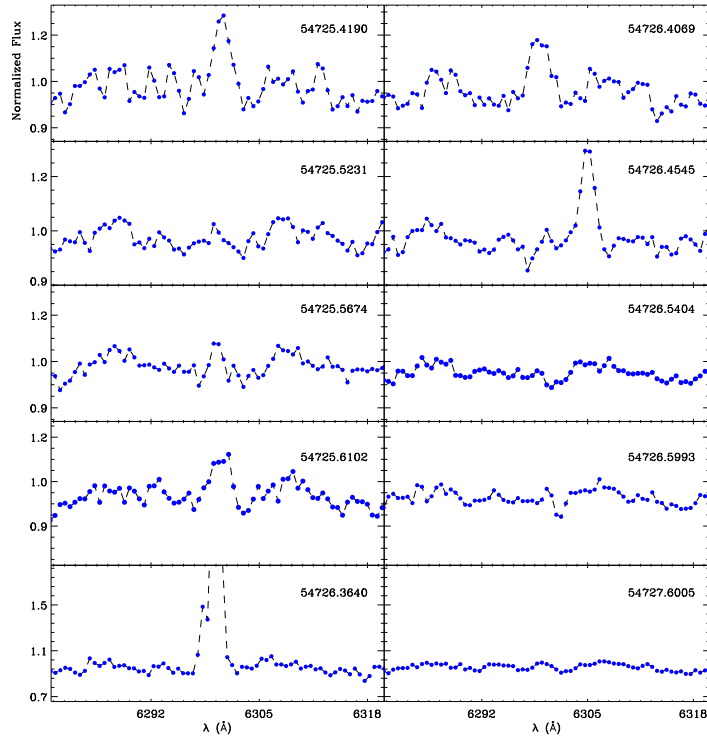


Figure 7. Variation of the forbidden emission line profiles of the [O I] at 6300 Å.

at phases of 0.4829 and 0.5973. The H_{α} emission line profile at orbital phase of 0.3996 has an unexpected shape because it is very resemblance of *inverse P Cygni profile*, most similar to UX Tau A (see Reipurth et al. 1996). The dramatic changes in the shape of the H_{α} line, collected on JD 2454727, are clearly seen in the last five panels of Fig. 6. The H_{α} line in the spectra of the NSVS 0650 taken at phases of about 0.2114, 0.3141 and 0.3772 displays blue-shifted absorption, similar to wTTS GG Tau (Folha & Emerson, 2001). It turns to be single absorption at orbital phases of 0.4610 and 0.5410.

The higher Balmer series, H_{β} and H_{γ} lines of NSVS 0650 generally appear to be in emission at all orbital phases. Again, dramatic line profile changes are evident. Inverse P Cygni profiles are also visible at some orbital phases.

The existence of blue-shifted absorption components in the Balmer lines of TTSs' spectra was first noted by Herbig (1962), who suggested that these absorption components are evidence for strong stellar winds. On the other hand Walker (1972) drew attention to the wTTSs which have red-shifted absorption in the higher-order Balmer lines. These inverse P Cygni profiles have generally been interpreted in terms of material accreting onto the young stars. The optical observations of unidentified Einstein Observatory X-ray satellite sources led to the discovery of many TTSs with weak H_{α} and IR excess emission (Strom et

al. 1990). The wTTSs have also dark spots as in the case of cTTSs but stronger X-ray in emission than cTTSs. They have also shallow or no disks. If a wTTS has still a disk some winds are blown away from this disk. Most TTSs are members of close binaries which may be born without a disk or have a short-lived disk (Neuhauser, 1997). Three types of binaries including TTS without disks, with circumstellar disks and with circumbinary disks exist.

4.2 Forbidden lines

One of the most important characteristics in the spectra of the cTTSs is the presence of forbidden emission lines. The forbidden neutral oxygen lines are not seen in the spectra of wTTSs. In the spectra of NSVS 0650 we observed forbidden [OI] emission line at 6300 Å. Figure 7 displays the [OI] emission line profiles at various orbital phases. [OI] emission line shows single peaks, but the line centroid is shifted to the blue. The strength of emission in [OI] 6300 Å is highly variable and seems to correlate with the orbital phase. This forbidden emission line appears to be slightly stronger at the first quadrature than at the second one. In the optical spectrum of cTTSs the forbidden emission lines are dominated. These lines are usually patterns of shocked low-density regions of young stars (Fernandez & Cameron 2001). These shocks can be produced by the outflowing materials, winds, and/or jets. Strong H_α and [OI] emission lines in the optical spectra of NSVS 0650 are indicative of ongoing accretion. The strength of H_β and its equivalent width (EW) seems to correlate well with that of H_α , as shown in Fig. 8. However the EWs of [OI] do not correlate well with those of the H_α , as is seen in the upper panel of Fig. 8. It appears that as if there is an anti-correlation between [OI] and H_α . The range of variation in the EWs of H_α is between about 2 Å and about -3 Å. Whereas the EWs of [OI] vary from 0 to about -1 Å. However, we observed the most strong emission in [OI] on JD 2454726.3640 at orbital phase of 0.1404 with an EW of -2.2 Å. We also measured the average EW of LiI as 0.3 ± 0.2 Å.

5 DISCUSSION

One of the goals of the present study is to derive the physical parameters of the low-mass stars in the eclipsing binary systems. As it is known eclipsing binaries are the most suitable laboratories for determining the fundamental properties of the stars and thus for testing the predictions of theoretical models. For this reason we started optical photometric and spectroscopic observations of some selected low-mass stars. We obtained multi-band light

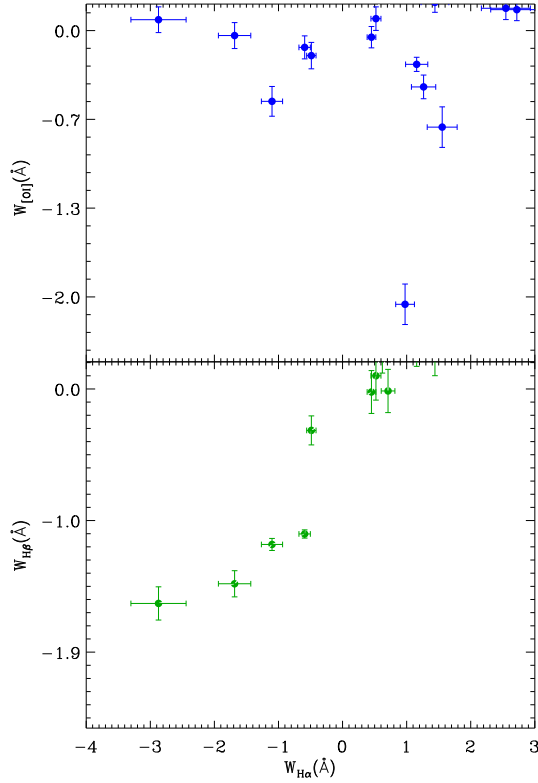


Figure 8. Correlations between equivalent width of the most prominent emission lines measured in the spectra.

Table 5. Fundamental parameters of the system.

Parameter	Primary	Secondary
Mass (M_{\odot})	0.656 ± 0.086	0.279 ± 0.045
Radius (R_{\odot})	0.600 ± 0.030	0.442 ± 0.024
$\log g$ (<i>cgs</i>)	4.699 ± 0.032	4.594 ± 0.047
T_{eff} (K)	3960 ± 80	3365 ± 80
$(v \sin i)_{calc.}$ (km s^{-1})	59 ± 3	43 ± 2
$\log (L/L_{\odot})$	-1.097 ± 0.057	-1.647 ± 0.062
d (pc)	111 ± 9	
J, H, K_s (mag)*	$10.918 \pm 0.032, 10.267 \pm 0.028, 10.092 \pm 0.025$	
$\mu_{\alpha}, \mu_{\delta}$ (mas yr^{-1})**	$23.70 \pm 6.10, 17.50 \pm 6.10$	
U, V, W (km s^{-1})	$-40 \pm 5, +19 \pm 4, -14 \pm 3$	

*2MASS All-Sky Point Source Catalogue (Cutri et al. 2003)

**NOMAD Catalog (Zacharias 2005)

curves and spectra with a wide wavelength range. We analyzed the V-, R-, and I-bandpass light curves and the radial velocities separately using the modern codes. Then, we combined the photometric and spectroscopic solutions and derived the absolute parameters of the component stars. The standard deviations of the parameters have been determined by JK TABSDIM¹ code, which calculates distance and other physical parameters using sev-

¹ This can be obtained from <http://http://www.astro.keele.ac.uk/~jkt/codes.html>

eral different sources of bolometric corrections (Southworth et al. 2005). The best fitting parameters are listed in Table 5 together with their formal standard deviations.

The luminosity and absolute bolometric magnitudes M_{bol} of the stars were computed from their effective temperatures and their radii. Since low-mass stars radiates more energy at the longer wavelengths we used $VRIJHK$ magnitudes given by Coughlin & Shaw (2007). Applying $BVRIJHKL$ magnitudes- T_{eff} relations given by Girardi (2002) we calculated the distance to NSVS 0650 as $d=111\pm 9$ pc. Estimating distances to low-mass stars are strongly depended on the bolometric corrections. If we adopt the bolometric corrections given by Siess, Forrestini & Dougados (1997) the distance to NSVS 0650 reduces to about $d=86\pm 4$ pc. The mean light contribution of the secondary star $L_2/(L_1+L_2)=0.22$ obtained directly from the I-bandpass light curve analysis is in a good agreement with that estimated from the bolometric luminosities as 0.22. This result indicates that the light contribution of the less massive component is very small, indicating its effect on the color at outside eclipse is very limited.

Locations of the primary and secondary components on the theoretical mass-radius and $T_{eff} - \log L/L_{\odot}$ diagrams are shown in Fig. 9. The mass tracks and isochrones are adopted from Siess, Forrestini & Dougados (1997) and Siess (2000). Since the stars appear to be in pre-main sequence evolution we adopted $Z=0.03$. These mass tracks are very close to those obtained for solar abundance. The radius of more massive primary component is in agreement with that zero-age main sequence star having the same mass. However, the secondary is about 35 % larger than the main-sequence counterpart. This result confirm the hypothesis proposed by Chabrier, Gallardo & Baraffe (2007) for the larger radius of the low-mass convective stars. The existence of Li 6708 Å absorption line in the spectra and comparison the absolute dimensions of the components with the evolutionary tracks may be taken as an indicator of the pre-main-sequence stars. The components of NSVS 0650 lie on the isochrones between 15-30 Myr, still in contracting phase toward the main-sequence. If we use the isochrones plotted M_v versus $B - V$ we estimate an age of about 10-15 Myr. This difference arises from the bolometric corrections given by Siess, Forrestini & Dougados (1997). We used the color-temperature calibrations given for the main-sequence stars for estimating the effective temperature of the more massive primary component. If we use the color-temperature relation given for luminosity class IV stars (de Jager and Nieuwenhuijzen, 1987) we find even smaller effective temperature of about 3700 K for the primary component. The difference of about 250 K in the effective temperature of the primary star shifts its location

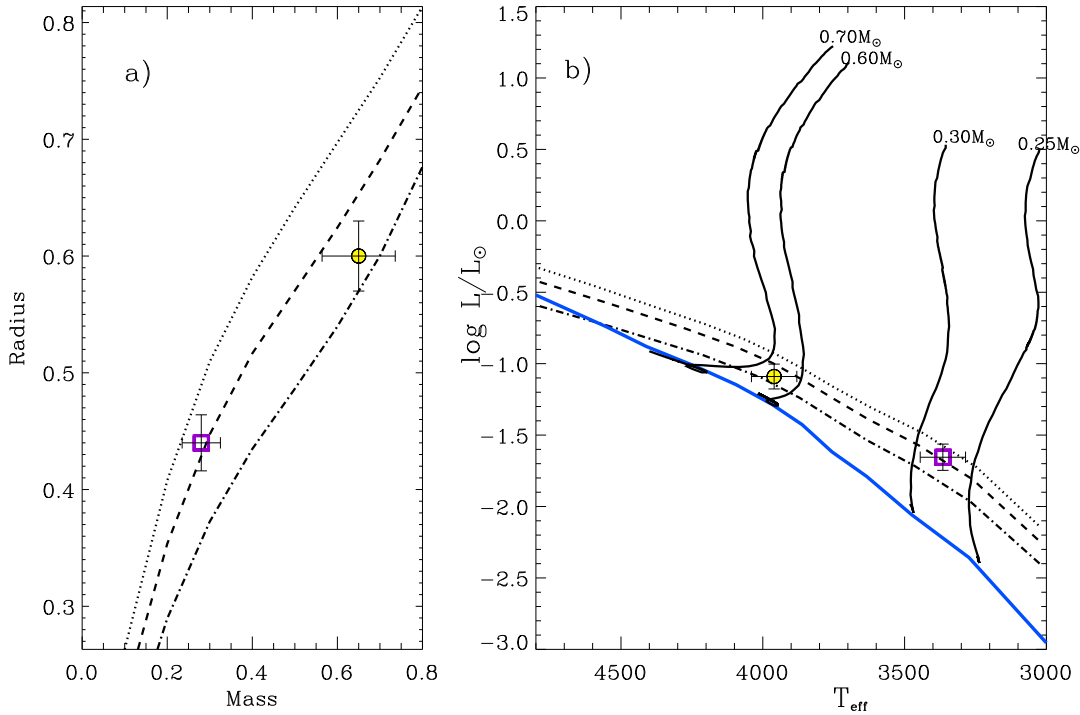


Figure 9. Comparison between stellar models and the absolute dimensions of NSVS 0650 in the mass-radius (a) and $T_{\text{eff}} - \log(L/L_{\odot})$ (b) planes. The mass-radius relations in panel (a) were derived using the stellar models of Siess et al. (2000) for $Z=0.03$ with an age of 15 (dotted), 20 (dashed) and 30 Myr (dot-dashed). Panel (b) shows the locations of the components in the HR diagram. Evolutionary tracks for the masses of 0.25, 0.30, 0.60 and 0.70 M_{\odot} are shown for comparison. The diagonal lines from left to right indicate isochrones with an age of 15 (dotted), 20 (dashed) and 30 Myr (dot-dashed) and zero-age main-sequence (continuous line). The filled-circle and square indicate the primary and secondary components of NSVS 0650, respectively.

to the lower-right in the HR diagram which corresponds to a smaller age. We estimate an age of about 50 Myr using the pre-main-sequence models given by D’Antona & Mazzetelli (1997), and 63 Myr by Baraffe et al. (1998) slightly larger than that given by Siess et al. model. The evolutionary models indicate that a star with a mass of 0.66 M_{\odot} takes about 100 Myr to contract and reach its normal main-sequence radius.

The LiI 6708 Å line is often used as an age indicator. In the spectra of NSVS 0650 the LiI line is clearly seen. Moreover, in the optical spectrum of the system, we observed also H_{α} and H_{β} lines as in emission. In addition, strong emission of the [OI] forbidden line is visible. These features are signs of cTTS but, in contrary, the measured EW values point a wTTS. The primary component of NSVS 0650 appears in the region of *Li-poor* stars located on the HR diagram (see Fig. 8 in Sestito, Palla & Randich, 2008). The measured EW of 0.3 Å for LiI is in agreement with this classification. High-resolution spectra are urgently required to confirm our finding and to derive which sub-group, cTTS or wTTS, it belongs.

6 ACKNOWLEDGEMENTS

The authors acknowledge generous allotments of observing time at TUBITAK National Observatory (TUG) of Turkey. We also wish to thank the Turkish Scientific and Technical Research Council for supporting this work through grant Nr. 108T210 and EBİLTEM Ege University Science Foundation Project No:08/BİL/0.27 . We have use of 2MASS USNO and NOMAD Catalogs as well as the Simbad, Visir, and ADS databases. The anonymous referee is gratefully acknowledged for useful and constructive suggestions.

REFERENCES

- Alcala J. M., Covino E., Franchini M., Krautter J., Terranegra L.; Wichmann R., 1993, 272, 225
- Alencar S. H. P., Basri G., 2000, AJ, 119, 1881
- Barrado y Navascues D. & Martin E. L., 2003, AJ, 126, 2997
- Baraffe I., Chabrier G., Allard F., Hauschildt P. H., 1998, A&A, 337, 403
- Bertout, C. et al. 2007, AA, 473, L21
- Chabrier G., Gallardo J., Baraffe I., 2007, A&A, 472, 17
- Coughlin J. L., and Shaw J. S., 2007, JSARA, 1, 7C
- Covino E., Terranegra L., Magazzu A., Alcala J. M., Allain S., Bouvier J., Krautter J., Wichmann R., ASPC, 109, 421
- Cutri R. M., et al., 2003, The IRSA *2MASS* All-Sky Point Source Catalog, NASA/IPAC Infrared Science Archive. <http://irsa.ipac.caltech.edu/applications/Gator/>
- D'Antona C., Mazzitelli A., 1997, ApJ, 477, 519
- Delfosse X., Tinney C. G., Forveille T. et al., 1997, A&A, 327L, 25D
- Drilling J. S., Landolt A. U., 2000, Allen's astrophysical quantities, 4th ed. Edited by Arthur N. Cox. ISBN: 0-387-98746-0. Publisher: New York: AIP Press; Springer, 2000, p.381
- de Jager C., Nieuwenhuijzen H., 1987, AAP, 177, 217
- Fernandez M., Cameron F., 2001, A&A, 380, 264
- Ferro A., Giridhar S., 2003, A&A, 408, 29
- Folha D. F. M. & Emerson J. P., A&A, 365, 90
- Girardi L., Bressan A., Bertelli G., and Chiosi C., 2002, A&AS, 141, 371
- Herbig G. H., 1962, Adv. in Astron. Astrphys., 1, 47

- Hernández J., Calvet N., Briceño C., Hartmann L., Berlind P., 2004, *AJ*, 127, 1682
- Kwee K. K., van Woerden H., (1956), *BAN*, 12, 327
- Lopez-Morales M. and Ribas I., 2005, *ApJ*, 631, 1120
- Lucy L. B., 1967, *Z. Astrophys.*, 65, 89
- Nidever D. L., Marcy G. W., Butler R. P., Fischer D. A., and Vogt S. S., 2002, *ApJS*, 141, 503
- Neuhauser R., 1997, *Science*, 276, 1363
- Prsa A. and Zwitter T., 2005, *ApJ* 628, 426
- Reipurth B., Nyman L.-A., Chini R., 1996, *A&A*, 314, 258
- Ribas I., 2003, *A&A*, 398, 239
- Shaw J. S., Lopez-Morales M., 2006, *ASPC*, 362, 15
- Schisano, E. et al. 2009, *AA*, 501, 1013
- Sestito P., Palla F., & Randich S., 2008, *A&A*, 487, 965
- Siess L., Forestini M., Dougados C., 1997, *A&A*, 325, 556
- Siess L., Dufour E., Forestini M., 2000, *A&A*, 358, 593
- Strom R. G., Croft S. K., Boyce J. M., 1990, *Science*, 250, 437
- Southworth J., Clausen J. V., 2005a, *A&A*, 461, 1077
- Skrutskie M. F. et al., 1999, *AJ*, 131, 1163
- Tokunaga A. T., 2000, "Allen's astrophysical quantities", Fourth Edition, ed. A.N.Cox (Springer), p.143
- Topping J., 1972, "Errors of Observation and Their Treatment", (Chapman and Hall Ltd.), p.89
- Tonry J. and Davis M., 1979, *AJ* 84, 1511
- van Hamme, W., 1993, *AJ*, 106, 2096
- Wozniak P. R. et al., 2004, *AJ*, 127, 2436
- West A. A., Hawley S. L., Walkowicz L. M., et al., 2004, *AJ*, 128, 426
- Wilson R.E. and Devinney E.J., 1971, *ApJ*, 166, 605
- Walker M. F., 1972, *ApJ*, 175, 89
- York D. G., Adelman J., Anderson J. E., et al., 2000, *AJ*, 120, 1579
- Zacharias N., Monet D. G., Levine S. E., 2004, *AAS*, 205, 4815Z